

# Optimal Landmark Selection for Registration of 4D Confocal Image Stacks in Arabidopsis

Katya Mkrtychyan, Anirban Chakraborty, and Amit Roy-Chowdhury

## Abstract

Technologically advanced imaging techniques have allowed us to generate and study the internal part of a tissue over time by capturing serial optical images that contain spatio-temporal slices of hundreds of tightly packed cells. Image registration of such live-imaging datasets of developing multicellular tissues is one of the essential components of all image analysis pipelines. In this paper, we present a fully automated 4D(X-Y-Z-T) registration method of live imaging stacks that takes care of both temporal and spatial misalignments. We present a novel landmark selection methodology where the shape features of individual cells are not of high quality and highly distinguishable. The proposed registration method finds the best image slice correspondence from consecutive image stacks to account for vertical growth in the tissue and the discrepancy in the choice of the starting focal point. Then it uses local graph-based approach to automatically find corresponding landmark pairs, and finally the registration parameters are used to register the entire image stack. The proposed registration algorithm combined with an existing tracking method is tested on multiple image stacks of tightly packed cells of Arabidopsis shoot apical meristem and the results show that it significantly improves the accuracy of cell lineages and division statistics.

## Index Terms

live cell imaging, confocal laser scanning microscopy, image registration, shoot apical meristem.



- 
- *K. Mkrtychyan is with the Department of Computer Science and Engineering, University of California, Riverside, Riverside, CA, 92521.*
  - *A. Chakraborty and A. Roy-Chowdhury are with the Department of Electrical and Computer Engineering, University of California, Riverside, Riverside, CA, 92521. E-mail: amitrc@ee.ucr.edu*

PROPER understanding of the causal relationship between cell growth patterns and gene expression dynamics is one of the major topics of interest in developmental biology. Information, such as rates and patterns of cell expansion and division, play a critical role in explaining cell growth and deformation dynamics. The need for quantification of these biological parameters and observing their evolution in time is very important. To achieve this goal, advanced microscopy techniques are used to collect time lapse videos and quantify the behavior of hundreds of cells in a tissue over multiple days. One of these techniques is the Confocal Laser Scanning Microscopy (CLSM) based Live Cell Imaging. This technique allows us to take optical cross sections of the cells in the tissue over multiple observational time points to generate spatio-temporal 4D (X-Y-Z-T) image stacks. To analyze the details of the collected image data, it is necessary to develop a fully automated image processing and analysis framework which gives rise to many new automated visual analysis challenges.

The image processing and analysis framework for gathering the cell growth and division statistics comprises of three main parts - image registration, cell segmentation and cell tracking. Without proper registration the subsequent parts in the image analysis system would fail. The misalignments present in the live imaging stacks are both temporal and spatial. The spatial shifts between images from different temporal stacks are caused from the involvement of manual *work* in noncontinuous imaging procedure (physically moving the specimen from one place to another). Note that because of the robustness of microscopy techniques the images in one spatial (X-Y-Z) stack are almost registered. But because of continuous growth of the living organism during the imaging procedure there is also a slice matching issue in consecutive stacks to be solved. The presence of the slice mismatch between image stacks and significant shifts between images prevent getting accurate cell tracking and cell division detection, which causes collection of non accurate statistics. That is why the issue of registration is very important.

As an example let us consider this scenario; 3D confocal laser scanning microscopy is used to capture 4D (depth/time) image stacks of 'Shoot Apical Meristem' (SAM) of the plant *Arabidopsis*. The SAM of *Arabidopsis Thaliana* consists of approximately 500 cells and they are organized into multiple cell layers that are clonally distinct from one another and are tightly packed with each other. At each imaging time there is no control over which depth of the meristem the imaging starts. Also at each imaging/observational time point the plant is moved and placed under microscope to acquire the images. Because of this replacement of the plant under the microscope and the lack of control on the imaging depth the 4D dataset contains unregistered image stacks. Figure 1 demonstrates three consecutive stacks imaged at three different depths where the the same depth slices do not correspond. The figure also demonstrates images with noticeable shifts between images from different time instances. Automated analysis of cell lineages, cell growth dynamics requires the 4D image stacks to be registered. We will show experimental results on this particular application setting.

## 1.1 Contribution

In this work we present a fully automated spatio-temporal registration framework for registering live imaging stacks. This framework is suitable across tissues which show the characteristic of having tightly packed cells.

We have provided an optimization based framework to select the best image slice correspondence from consecutive image stacks by using the tissue characteristics in images. Also we have presented a novel landmark selection methodology where the shape features of individual cells are not of high quality and often non-discriminative. We solved the problem by choosing the relative positions and ordered orientation of the neighboring cells as unique features. We represented the local neighborhood structures of cells as graphs and selected those landmark points that have the minimum distance between the local graphs built around them.

A preliminary version of this work was presented in [10] where we assumed that the slice correspondences between Z-stacks were given. In [10] the input comprised of any two confocal image slices from two Z-stacks. The method proposed in this paper is a truly automated 4D registration method as the input to this method is a complete time lapse confocal image stack. Finding the corresponding slices needed to register is a big step in order to scale the problem and it is a fundamental problem that we are addressing in this work. Also we are looking at how the choice of the stack is reflected in the registration problem. Our analysis, presented in (Figure 6), shows the fundamental effect of a proper slice selection on the registration and subsequent image analysis results. We have shown the effect of using optimal image slice correspondences in the registration module and the improvements in results are evident in Figure 6. As explained in the Section 3, there is a significant increase in number of tracked cells and lengths of cell lineages, which validates the use of the slice correspondence method in the registration framework.

Also, we have improved the theoretical side of the landmark selection method over [10] by forcing a constraint into the optimization. It was done to insure feasibility on the selected set of landmark point pairs. The reason behind this change is that the rotation is governed by the rotation of the tissue, the cell independently cannot rotate by different amounts.

To show the significance of the registration and to show that our proposed registration method provides good results we considered the CLSM image stacks of tightly packed cells of a live Arabidopsis shoot meristem (SAM) (the spatio-temporal misalignments present in the sample CLSM image stack of a Arabidopsis shoot meristem are shown in Figure 1). We combined our proposed registration method with *local-graph matching* based robust cell tracking algorithm [2] and show significant improvement in accuracy of cell lineages and division statistics.

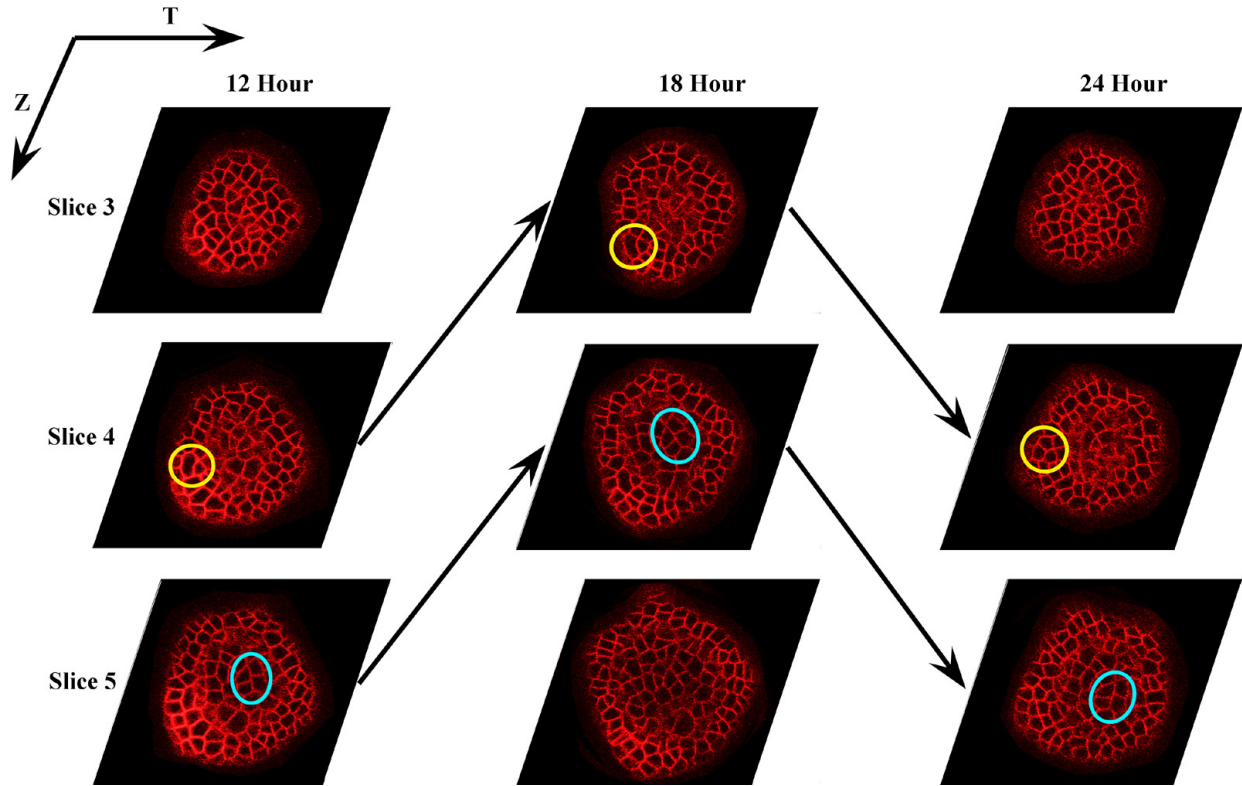


Fig. 1. Three consecutive Z-stacks with three consecutive slices shown. The black arrows between images show the slice correspondence between Z-stacks. The same color circles show the same collection of cells through the spatio-temporal slices.

## 1.2 Relation to Existing Work

Amongst the different components of the general image analysis pipeline there has been some work done on image segmentation and cell tracking in live imaging stacks. For cell segmentation, both the Watershed [5] and the Level-set method [4] have been shown to provide good results. In general, any segmentation method, e.g. [20], [21], can be used as a preprocessing step. Many tracking methods have been proposed that attempt to find correspondences between 2D segmented cells. For example, [2] exploits the local geometric structures around a cell to find correspondences between cells. [9] integrates the segmentation and tracking modules to reach an optimized segmentation and tracking result. In [8] multiangle image acquisition, three-dimensional reconstruction and cell segmentation lineage tracking approach is developed in which SAM is imaged from

multiple angles. But all of these methods rely on the availability of registered image stacks of the tissue.

In many works e.g. [2], [9], [13], [14], [15], [16], the images are registered with maximization of the mutual information method [1]. But this method may not be always effective. For example, we have looked at the confocal imagery of the Arabidopsis SAM for experiments in this paper. The mutual information based tracker fails to perform satisfactorily as it uses the pixel intensities to acquire the registration. Pixel intensities in the Arabidopsis SAM images are not discriminative features. The landmark-based registration is more suitable for noisy and Z-sparse confocal images than registration based on maximization of the mutual information, which we demonstrate in the experimental results section.

A recent paper [8] uses SAM images acquired from multiple angles to automate tracking and modeling. In this work, for pair of images to be registered, the user identified correspondences by pairing a few anchor points (referred as landmark points in this work). In this work, we present a fully automated method to find the corresponding temporal slices from Z-stacks of images and a fully automated landmark-based registration method that can find out correspondences between two images and utilize these correspondences to yield a better registration result. This method is suitable across tissues which show the characteristic of having tightly packed cells.

A commonly used landmark-based registration algorithm is the Iterative Closest Point algorithm [6], which is very sensitive to initialization. There are number of subsequent variations of this algorithm, e.g. Iterative Closest Point using Invariant Features [7], which uses features like eccentricity and curvature to overcome the issue. There are other registration works [17], [18] that acquire the registration using features like intensity, surfaces, and SIFT. But in tissues (e.g. Arabidopsis SAM) that are comprised of tightly packed cells with stereotypical shapes and sizes, eccentricity and other common features are not discriminative enough to be used for the selection of landmarks for

registration. This is why we need to develop a novel feature to register this type of images. The novel landmark estimation method presented in this paper exploits the tight spatial topology of the tissues under study and proposes a feature descriptor based on the local neighborhood structure around a cell for a robust registration method.

### 1.3 Organization

The rest of the paper is organized as follows. The algorithmic details of the proposed framework; finding the best image slices correspondence, feature matching in the selected images and entire Z-stack registration are provided in Section 2. We have shown experimental results and validation of our approach in Section 3 followed by concluding discussion in Section 4.

## 2 DETAILED REGISTRATION FRAMEWORK

The spatio-temporal registration of live imaging stacks comprises of three major steps: finding corresponding image slices from two consecutive image stacks, feature matching in the selected corresponding images, and aligning two stacks of images.

The next three sections present details of each step of the registration.

### 2.1 Finding Corresponding Temporal Slices

In most cases, for any two Z-stacks imaged at consecutive time intervals, the same depth image slices will not correspond. We consider all slice pairings between two consecutive Z-stacks and define distance on each pair correspondence. The distances are computed based on the tissue characteristics in images. Specifically the number of cells and the area of the tissue in the image are used to compute the distance.

Let us consider two consecutive Z-stacks  $I^{(t)}$  and  $I^{(t+1)}$  taken at time  $t$  and  $t + 1$ . The image  $i$  corresponds to the confocal slice image taken at time  $t$  and at the depth  $h_i \mu\text{m}$  and image  $j$ , corresponds to the confocal slice image taken at time  $t + 1$  and at the depth

$h_j$   $\mu\text{m}$ . Let  $n_i^{(t)}$  and  $n_j^{(t+1)}$  be the number of cells and let  $a_i^{(t)}$  and  $a_j^{(t+1)}$  be the area of the tissue in images  $i$  and  $j$ , taken at time  $t$  and  $t + 1$  respectively. We define the distance for the image pair  $(i, j)$  to be the best pair candidate as  $d(i, j)$  the following way:

$$d(i, j) = \frac{|n_i^{(t)} - n_j^{(t+1)}|}{n_i^{(t)} + n_j^{(t+1)}} + \frac{|a_i^{(t)} - a_j^{(t+1)}|}{a_i^{(t)} + a_j^{(t+1)}} \quad (1)$$

The constructed distance matrix  $d$  will contain distance values for all possible pairs between the two Z-stacks. We can see from the way the distances are computed that the smaller the distance corresponding to the image pair is the better image slice candidate the pair is. So the final slice correspondence between consecutive Z-stacks  $I_i^{(t)}$  and  $I_j^{(t+1)}$  is defined as:

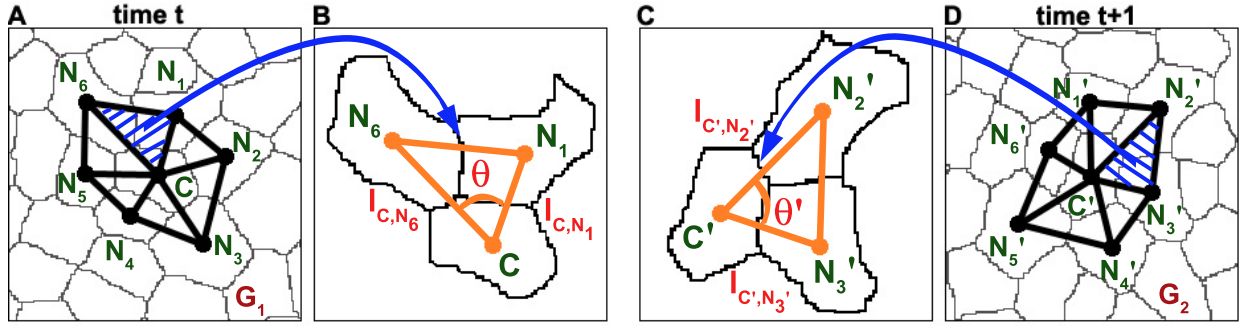
$$(i, j) = \arg \min_{i \in I^{(t)}, j \in I^{(t+1)}} d(i, j) \quad (2)$$

Essentially, the above described problem of finding corresponding slices is analogous to the shortest path problem [11], which is to find a path between two vertices (nodes) in a graph such that the sum of the weights of its constituent edges is minimized, where in our case every slice becomes a node. So the problem of finding corresponding temporal slices from the Z-stacks can be posed as a shortest path algorithm and can be solved using Dijkstra's algorithm [12], where the shortest path is only in temporal direction.

## 2.2 Feature Matching in Selected Images

Assuming that the best image slices between two Z-stacks are chosen, we want to find the features that can be used to find corresponding landmark point pairs to register one image stack onto the other.

When using landmark-based registration method, the quality of the image registration result depends on the accuracy of the choice of the landmark points. Finding corresponding landmark point pairs from two images depends on the feature selection. Motivated by the idea presented in [2], we use the relative positions and ordered orientation of the neighboring cells as unique features. To exploit these properties we



(A) The local graph  $G_1$  at time  $t$  with the central cell  $C$  and clockwise ordered neighboring cell vertices  $N_1, N_2, \dots, N_6$   
 (B) The local graph  $G_2$  at time  $t + 1$  with the central cell  $C'$  and clockwise ordered neighboring cell vertices  $N'_1, N'_2, \dots, N'_6$   
 (C) Triangle subgraph of the graph  $G_1$  with features  
 $N_{i_1}, N_{i_2} - i_1^{th}$  and  $i_2^{th}$  neighboring cells of  $C$   
 $\theta_{N_{i_1}, C, N_{i_2}}$  - angle between  $\overline{N_{i_1}C}$  and  $\overline{N_{i_2}C}$   
 $l_{C, N_{i_1}}(t), l_{C, N_{i_2}}(t)$  - neighbor edge lengths  
 $A_{N_{i_1}}(t), A_{N_{i_2}}(t)$  - areas of the cells  $N_{i_1}, N_{i_2}$   
 (D) Triangle subgraph of the graph  $G_2$  with features  
 $N'_{j_1}, N'_{j_2} - j_1^{th}$  and  $j_2^{th}$  neighboring cells of  $C'$   
 $\theta_{N'_{j_1}, C', N'_{j_2}}$  - angle between  $\overline{N'_{j_1}C'}$  and  $\overline{N'_{j_2}C'}$   
 $l_{C', N'_{j_1}}(t + 1), l_{C', N'_{j_2}}(t + 1)$  - neighbor edge lengths  
 $A_{N'_{j_1}}(t + 1), A_{N'_{j_2}}(t + 1)$  - areas of the cells  $N'_{j_1}, N'_{j_2}$

Fig. 2. Local graphs and two enlarged triangle subgraphs with indicated features.

represent these local neighborhood structures as graphs and select the best candidate landmark points that have the minimum distance between the local graphs built around them.

### 2.2.1 Local Graphs as features

Graphical abstraction is created on the collection of cells. Vertices in the graph are the centers of the cells and neighboring vertices are connected by an edge. Neighborhood set  $N(C)$  of a cell  $C$  contains the set of cells that share a boundary with  $C$ . Thus every graph consists of a cell  $C$  and a set of clockwise ordered neighboring cells (Figure 2 (A,D)). The ordering of the cells in  $N(C)$  is important because under non-reflective similarity transformation, the absolute positions of the neighboring cells could change but the cyclic order of the cells remains invariant.

### 2.2.2 Landmark point pair estimation from local graphs

Cell divisions happen throughout the entire imaging period but at the consecutive images only a few cell divisions are present. Ideally, in the areas where there is no

cell division, the local graph topology should not change (segmentation errors will circumvent this in practice). We exploit these conditions to find the corresponding landmark pairs in two images. Let  $G_1^{(t)}$  and  $G_2^{(t+1)}$  be two local graphs constructed around the cells  $C$  and  $C'$  in consecutive temporal slices (Figure 2). For each subgraph of the local graph  $G(t)$ , we define feature vector the following way;

$$\begin{aligned}
 F^C(t) &= [f_1 f_2 f_3 f_4 f_5]^T, \text{ where} \\
 f_1 &= \theta_{N_{i_1}, C, N_{i_2}}(t), \\
 f_2 &= l_{C, N_{i_1}}(t), f_3 = l_{C, N_{i_2}}(t), \\
 f_4 &= A_{N_{i_1}}(t), f_5 = A_{N_{i_2}}(t)
 \end{aligned}$$

We define the distance between two triangle subgraphs as

$$\begin{aligned}
 D_{TS}(F_i^C(t), (F_j^{C'}(t+1))) &= \sum_{k=1}^5 \left( \frac{f_k - f'_k}{f_k} \right)^2, \\
 \text{where } f_k &\in F_i^C(t), f'_k \in F_j^{C'}(t+1).
 \end{aligned} \tag{3}$$

To ensure that our landmark estimation method takes care of the rotation of the local area, we consider all cyclic permutations of the clockwise ordered neighbor set  $\{N'_1, N'_2, \dots, N'_m\}$  of the cell  $C'$  from the input image. The cyclic permutations of the set  $\{x_1, x_2, \dots, x_m\}$  can be written in terms of the shift  $k$  ( $k = 0, 1, \dots, (m-1)$ ) as the set  $\{x_{(1+k-1) \bmod(m)+1}, x_{(2+k-1) \bmod(m)+1}, \dots, x_{(m+k-1) \bmod(m)+1}\}$ . As an example, if  $(1, 2, 3)$  is the given sequence, then possible values of the shift  $k = 0, 1, 2$  and all the cyclic permutations of the sequence  $(1, 2, 3)$  will be  $(1, 2, 3), (2, 3, 1), (3, 1, 2)$  for  $k = 0, 1, 2$ . We consider all cyclic permutations of the clockwise ordered neighbor set  $\{N'_1, N'_2, \dots, N'_m\}$  of the cell  $C'$  from the input image and define the distance  $D(G_1, G_2^k)$  between two local graphs  $G_1$  and  $G_2$  based on the chosen permutation corresponding to shift  $k$  as

$$\begin{aligned}
 D(G_1, G_2^k) &= \sum_{\{i,j\}} D_{TS}(F_i^C(t), (F_j^{C'}(t+1))) \\
 \forall i \in \{1, 2, \dots, m\}, \quad j &= [(i+k-1) \bmod(m) + 1]
 \end{aligned} \tag{4}$$

for  $k \in \{0, 1, 2, \dots, (m-1)\}$ . We compute the sum of the distances between each of the

ordered pairs of triangle-subgraphs for each permutation  $k$ .

It is important to notice that in the calculation of the distance  $d(i, j)$  (Eqn. 1), which is used to find corresponding temporal slices, feature vector  $F$ , which is part of landmark point pair estimation, is not used. The reason is that the image stack slices are very stereotypical; there can be different local graph patterns which can be similar in shape but be from different slices. In confocal imaging a cell is imaged in multiple  $Z$  slices along time. This may result in having all cells in a cluster of tightly packed cells being imaged at slices  $z, z + 1, z + 2$  and at time points  $t$  and  $t + 1$ . If we want to use this micro feature  $F$  to choose the corresponding temporal slices, essentially there is a discrimination why slice  $z$  at time point  $t$  should match with slice  $z$  at time point  $t + 1$ . Because there is no difference in the cell cluster, it is equally possible that slice  $z$  at time point  $t$  can also match with slice  $z + 1$  at time point  $t + 1$ . This feature vector  $F$  is kind of invariant across  $Z$ , it discriminates cells spatially in one slice along time but it is not a discriminative enough feature to understand which slice should match to which slice as the same local graph (cell cluster) may be preserved along different depths. So these components of the feature vector  $F$  are micro level features and they do not capture the slice information. That is the reason why  $F$  does not capture the effect of the depth at which the cells are imaged and is not used to find the corresponding temporal slices.

The minimum distance  $D^*(G_1, G_2)$  between two graphs  $G_1$  and  $G_2$  corresponding to cells  $(C, C')$  for all permutations  $k$  is

$$D^*(G_1, G_2) = \min D(G_1, G_2^k) \quad (5)$$

where  $k \in \{0, 1, \dots, (m - 1)\}$ . This guarantees that our landmark estimation method is invariant of the rotation in the local area.

For all cell pairs  $C_i, C'_j$  and corresponding graphs  $G_i, G_j$  from two consecutive images, we compute the distance  $D^*(G_i, G_j)$ . Now, our objective is to obtain the set of best  $q$  cell pairs for which the local graphs around these cell pairs are maximally similar.

However, for each of these chosen cell pairs, the optimal shift (corresponding to the minimum distances between the graphs) must result in approximately similar angles of rotation. This uniformity between the rotation of the individual graphs is obvious as all the cells are tightly packed and the rotations of individual cell clusters (the ‘local graphs’) are uniformly affected by the global rotation of the entire tissue. Thus, as a corollary, if any set of  $q$  cell pairs show large variations in the optimum angle of rotation, the set must contain one or more incorrectly associated local graph pairs.

### 2.2.3 Measurement of Angle of Rotation Between Pairs of Graphs

Between two graphs  $G_1$  and  $G_2$ , the circular shift  $k^*$  corresponding to the minimum distance  $D^*(G_1, G_2)$  is given as,

$$k^* = \arg \min_k D(G_1, G_2^k) \quad (6)$$

Assuming that the rotated graph  $G_2^{k^*}$  is a candidate match for the graph  $G_1$ , the angle of rotation  $\Theta^*(G_1, G_2) = \Theta(G_1, G_2^{k^*})$  could be computed as follows.

Let in graph  $G_1$ , the central cell is  $C$  and the set of neighboring cell slices around  $C$  being  $\{N_1, N_2, \dots, N_m\}$ . Likewise, the central cell in the graph  $G_2$  is  $C'$  and the neighbors around it are  $\{N'_1, N'_2, \dots, N'_m\}$ . Now, if  $G_2^{k^*}$  is the transformed version of  $G_2$ , then the amount of rotation would be obtained as,

$$\Theta(G_1, G_2^{k^*}) = \frac{1}{2\pi} \left( \theta_{N'_{k^*+1}, C', Y'} - \theta_{N_1, C, Y} \right) \quad (7)$$

The angles  $\theta_{N_1, C, Y}$  and  $\theta_{N'_{k^*+1}, C', Y'}$  are described through Figure 3. The angle  $\Theta(G_1, G_2^{k^*})$  represents the amount of counterclockwise rotation that  $G_2$  must undergo with respect to  $C'$  to align  $\overline{N'_{k^*+1}C'}$  with  $\overline{N_1C}$  in  $G_1$ .

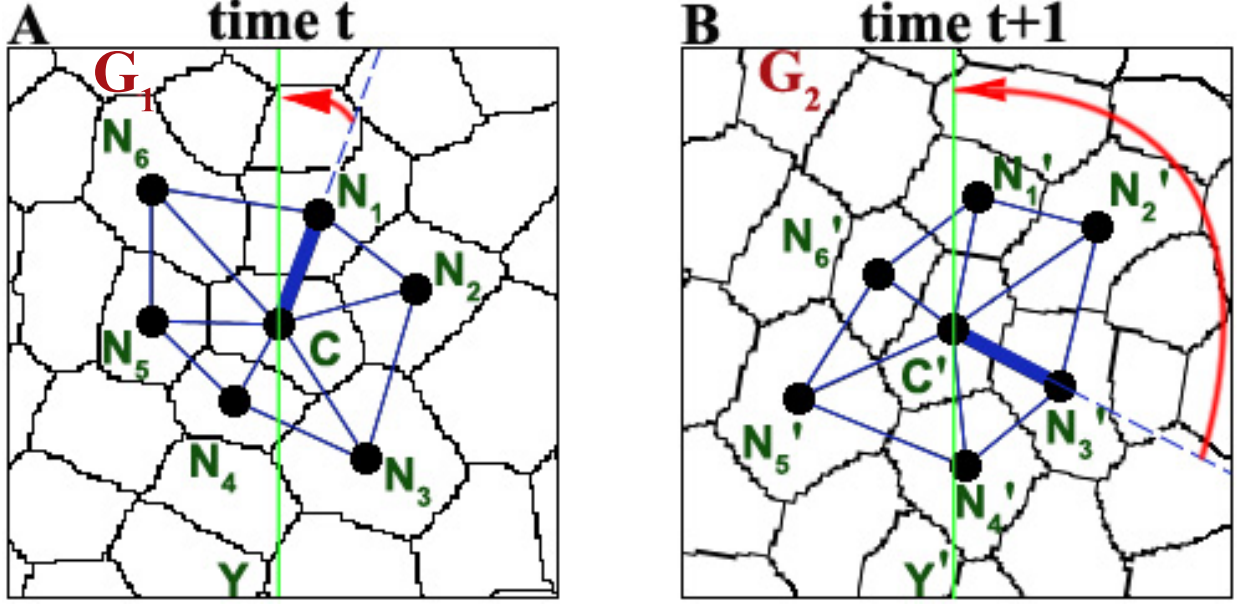


Fig. 3. Measuring the angle of rotation of a local graph. (A) A cell cluster at any given time instant  $t$ , centered around the cell  $C$ . The neighboring cells  $N_1, \dots, N_6$ , along with the central cell  $C$  constitutes the nodes of the local graph  $G_1$ . (B) The same cell cluster at time  $t + 1$ . The graph  $G_2$  is a rotated version of  $G_1$ . The optimum shift ( $k^*$ ) is estimated as 2 and hence  $\overline{N_1C}$  is rotated clockwise to  $\overline{N_3'C'}$  in  $G_2$ . Therefore, the relative normalized angle of rotation between  $G_1$  and  $G_2$  can be computed as  $\Theta^*(G_1, G_2) = \frac{1}{2\pi} (\theta_{N_3',C',Y'} - \theta_{N_1,C,Y})$ .

#### 2.2.4 Optimum Set of Landmarks: Simultaneously Minimizing Dissimilarities And Variance In Angles of Rotation Between The Local Graphs

The final objective is to obtain a set of  $q$  cell pairs from the two image slices such that the individual pairs of local graphs around those slices are maximally similar as well as the variation in the angles of rotation in this set is least. This set, denoted as  $s_q^* = \{(G_{i_1}, G_{j_1}^{k_1^*}), (G_{i_2}, G_{j_2}^{k_2^*}), \dots, (G_{i_q}, G_{j_q}^{k_q^*})\}$ , is the set of landmark pairs required for registration of the image pairs, where the individual landmarks are the centroids of the 2D cell slices.

Let the superset of all such possible  $q$ -pairs be  $\{s_q^1, s_q^2, \dots, s_q^V\}$ , and let it be denoted by  $\mathcal{S}$ . For any candidate set for landmarks  $s_q^l \subset \mathcal{S} \forall l = 1, 2, \dots, V$ , the average normalized dissimilarity between all pairs of local graphs in this set would be,

$$\overline{D}_l^* = \frac{1}{q} \sum_{(G_1, G_2) \in s_q^l} \frac{D^*(G_1, G_2)}{D_{max}^l} \quad (8)$$

where,  $D_{max}^l = \max D^*(G_1, G_2) \forall (G_1, G_2) \in s_q^l$ . The normalization is done to scale the average value between 0 and 1.

The variance in the angles of rotation over the set  $s_q^l$  is computed as,

$$\bar{\sigma}_{\Theta,l}^2 = \frac{1}{q} \sum_{(G_1, G_2) \in s_q^l} \Theta^*(G_1, G_2)^2 - \left( \frac{1}{q} \sum_{(G_1, G_2) \in s_q^l} \Theta^*(G_1, G_2) \right)^2 \quad (9)$$

The overall cost function is defined as a weighted sum of  $\bar{D}_l^*$  and  $\bar{\sigma}_{\Theta,l}^2$  and the best set of  $q$  landmark pairs is estimated by minimizing this cost function.

$$s_q^* = \arg \min_{s_q^l \in \mathcal{S}} \left\{ w \bar{D}_l^* + (1 - w) \bar{\sigma}_{\Theta,l}^2 \right\} \quad (10)$$

The weight  $w$  can be user-defined. Since the feature distance is the main parameter in finding the landmark point pairs, we varied the value of  $w$  between 0.5 and 1. The registration results were not changed. For all our experiments, the  $w$  is fixed at 0.5. The choice of  $q$  is described later in the Section 2.3.

Once we have the landmark point pairs, the positions of the landmark pairs in the two images are used to estimate the parameters of the transformation model (affine, non-reflective similarity etc.). Then the estimated transformation function maps the rest of the points in the input image to the reference image. The Section 2.3 presents details on computing the spatial transformation between the images and final image registration.

### 2.3 Image Registration

After the corresponding image slices across two stacks of images taken at two consecutive time points are selected and the corresponding landmark point pairs in the selected images are acquired, we find the spatial transformation between these images. Then we use the estimated transformation to register the entire Z-stacks.

### *2.3.1 Finding the spatial transformation between two images*

Once we have the landmark point pairs corresponding to the input (the image that we wish to transform) and reference (the image against which we want to register the input) images, we find the spatial transformation between them. Transformations present in the live image stack of a multilayer, multicellular structure where the cells are tightly packed together, include a rotation and a translation. The non-reflective similarity transformation is chosen as a type of transformation to proceed with. Finding the nonreflective similarity transformation between two images is a problem of solving a set of two linear equations. For better accuracy of transformation parameters the top  $q$  landmark point pairs are used in a least square parameter estimation framework. But, as known, greater the number of landmark point pairs is, better the estimated solution of the Least Square technique is. In order to choose the best landmark point pairs we rank them according to the similarity of local graphs created on the neighboring cell structure. Choosing more landmark points will mean finding transformation between two images based on points that have less possibility to be correct corresponding points, which will eventually lead to bad registration. So there is a trade-off between these aspects. In our experiments we choose four, five or six landmark point pairs depending on the CLSM dataset image quality.

### *2.3.2 Z-stack Registration*

Depending on the procedure the living tissue imaging is done, the transformations between corresponding image slices from consecutive image stacks are the same. So the transformation parameters corresponding to the selected image slices from these Z-stacks will also be the transformation parameters between the rest of the image pairs in these two Z-stacks. So, by applying the computed transformation parameters for the selected image slices on the rest of the image pairs from the two Z-stacks, the entire Z-stack taken at time point  $t + 1$  will be registered to the Z-stack taken at time point  $t$ .

### 3 EXPERIMENTAL RESULTS

#### 3.1 Imaging Setup

For the experiments performed in the present study, the 3D structure of the tissues are imaged using single-photon confocal laser scanning microscope and we have specially dealt with the 'Shoot Apical Meristem' (SAM) of the plant *Arabidopsis*. The SAM of *Arabidopsis Thaliana* consists of approximately 500 cells and they are organized into multiple cell layers that are clonally distinct from one another and are tightly packed with each other. By changing the depth of the focal plane, CLSM can provide infocus images from various depths of the specimen. To visualize cell boundaries of all the cells in the SAM, plasma membrane-localized Yellow Fluorescent Protein (YFP) is used. The set of images, thus obtained at each time point, constitute a 3-D stack, also known as the 'Z-stack'. Each Z-stack is imaged at a certain time interval (e.g. 3 or 6 hours between successive observations) and it is comprised of a series of optical cross sections of SAMs that are separated by approx.  $1.5 \mu\text{m}$ , and a standard shoot apical meristematic cell has a diameter of about 5 - 6  $\mu\text{m}$ .

At each imaging time there is no control over in which depth of the meristem the imaging starts, so in each Z-stack the first slice imaged is at random depth and the rest of the images in the stack are  $1.5\mu\text{m}$  deep from each other. This means that for any two Z-stacks imaged at consecutive time intervals, in most cases, the same depth slices of the specimen won't correspond, there will be a shift in the slice correspondence. Figure 1 demonstrates three consecutive stacks imaged at three different depths where the the same depth slices do not correspond.

In practice, the live cell imaging of *Arabidopsis* SAM comprises of several steps, where the plant has to be physically moved between different places. For normal growth of the plant, it has to be kept in a place having specific physical conditions (such as a temperature of  $24^{\circ}\text{C}$ ). The plant is moved and placed under microscope at the imaging/observational time points, before it is placed back to the aforementioned place

once again. For 72 hours overall, this process is repeated every 3 hours. Because of this process of replacement of the plant under the microscope and also since the plant keeps growing during these 72 hours, various shifts can occur between two Z-stacks of images taken in consecutive time points, though images in any Z-stack are automatically registered. Figure 1 demonstrates images from a data set with noticeable shifts between images from different time instances.

### 3.2 Experimental Results and Analysis

We further evaluate the performance of the proposed automatic spatio-temporal registration and show numerical results. As the numerical results as direct comparison of registration results are not trivial we evaluate the tracking accuracy after and before registration and show the performance improvement.

We have tested our proposed automatic spatio-temporal registration of live imaging stacks method on different datasets that consist of 4D image stacks taken at six hour intervals for 72 hours overall. First for each two consecutive Z-stacks of every dataset, we run our method to find the corresponding image slices. Then using the image correspondence information from corresponding Z-stacks we chose a temporal stack and applied the watershed segmentation [5] and local graph matching based tracking [2] methods and compared the obtained results. We compared tracking results of the proposed method with results obtained without registration, with semi-automated registration (the landmark pairs are chosen manually, the transformation is obtained automatically) and with Matlab registration module which is based on the maximization of the mutual information.

**Pairwise Tracking** - Figure 4 (A-E) shows cell tracking results from two consecutive images ( $30^{th}$  and  $36^{th}$  hour), obtained with different approaches. We can see that for the chosen two consecutive images ( $30^{th}$  and  $36^{th}$  hour) the results with maximization of the mutual information based registration and without registration show incorrect

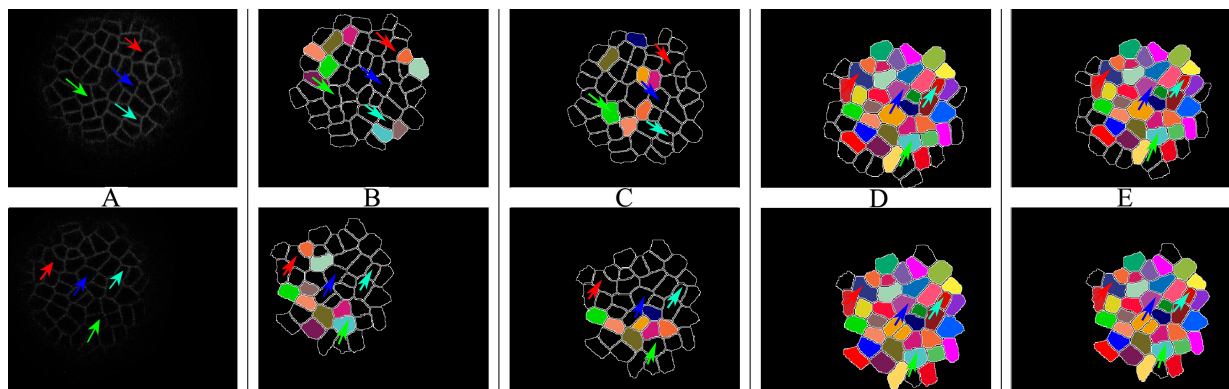


Fig. 4. A) Raw consecutive images (the same color arrows represent the same cells). Tracking results obtained B) without registration C) with registration based on maximization of the mutual information, D) with semi-automated registration (the landmark pairs are chosen manually, the transformation is obtained automatically), E) with proposed automatic registration. The same colors represent the same cell.

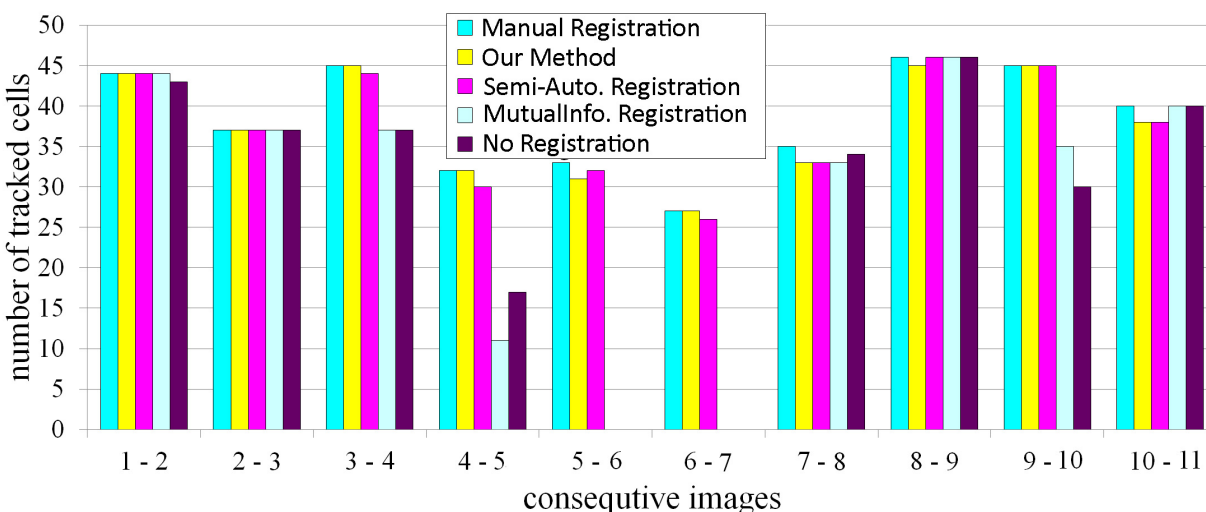


Fig. 5. Number of tracked cells across two consecutive images.

cell tracks. Whereas the proposed method and semi-automated registration correctly registered two images with 100% correct tracking results. Detailed results for the same dataset are shown in Figure 5. We can see that from 33 and 27 cells, present in the images at time points 5 (30<sup>th</sup> hour) to 6 (36<sup>th</sup> hour) respectively, none are tracked by the tracker run on the images registered with the registration based on the maximization of the mutual information and not registered images (as in Figure 4 (A-E)). The same result is seen for the tracking results in images at time points 6 to 7. But the tracking results obtained with proposed and semi-automated methods provided very close to manual

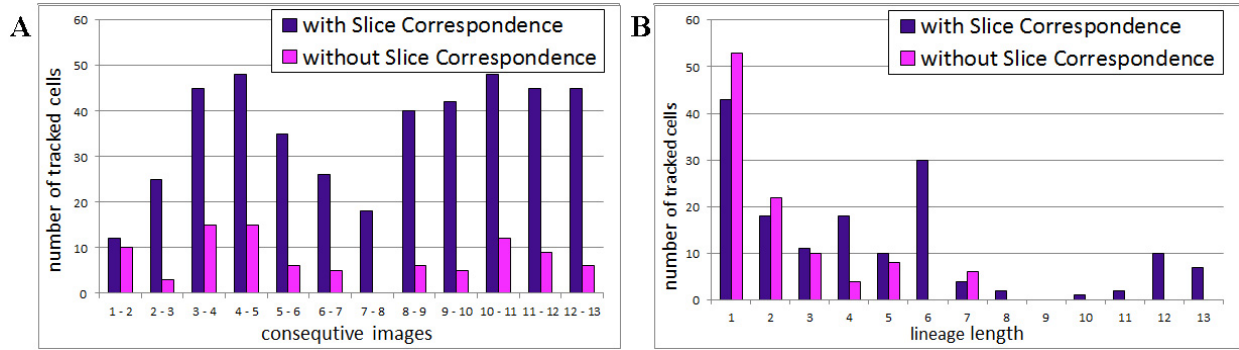


Fig. 6. Tracking results on a temporal image stack where the images are chosen from the Z-stacks based on the proposed slice correspondence and where the same slice is chosen from all Z-stacks - A) Number of tracked cells across two consecutive images, B) Length of cell lineages.

results.

**Image Slice Correspondence** Figure 6 shows two different tracking result comparisons on a temporal stack between the case where the temporal stack is constructed from the proposed automated image slice correspondence module and the case where from each Z-stack the same slice image is chosen. Figure 6 A) shows the number of tracked cells across each two consecutive images in the temporal stack and Figure 6 B) shows the lengths of cell lineages (for how many consecutive frames the same cell was tracked). All of these results are manually verified. We can see significant increase in number of tracked cells and lengths of cell lineages in the case where the dataset is constructed from our proposed image slice correspondence module which validates the use of the slice correspondence module in the registration framework.

**Pairwise Registration** - The result of the registration depends on the clearness of the images. Although, in the proposed method, we need very few landmark points we cannot control the regions of the images in which the landmark points may appear, so in the process of the selection of the landmark points we might take false positive landmarks which will result in pure registration. Figure 7 shows three pairwise registration results with images from three different depths, with different SNRs. As we can see the column A) in the figure shows three different images taken at hour 18 with different SNRs sorted from image with high to low SNR accordingly. Images in the column B) are registered

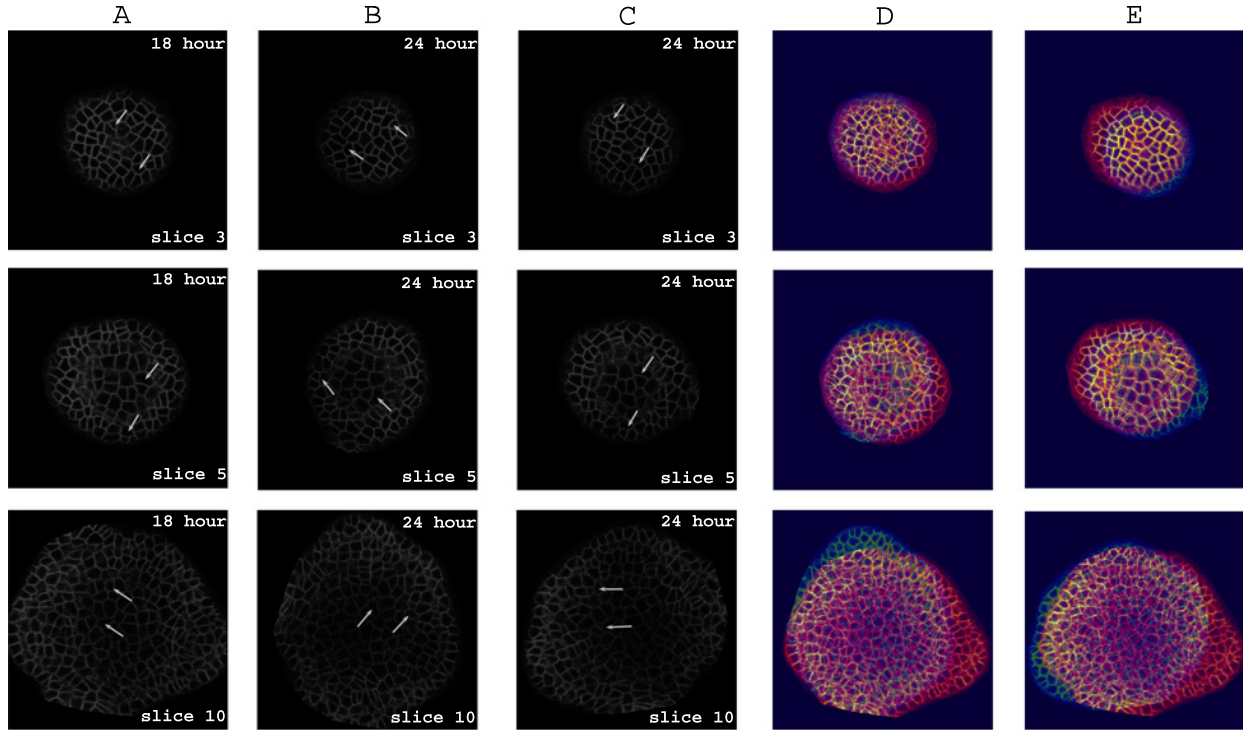


Fig. 7. Registration results on three pairwise images from three different depths and with different SNRs. Column A), B) show the raw images from the hour 18 and 24 correspondingly, column C) shows the image in the column B) after registration, and column D) and E) show the fused images before registration and after registration (white arrows show the same cells)

to the images in the column A) accordingly and column C) shows the same image after registration. As the white arrows in the figure show we have registration with high tracking error in the images from the first row (high SNR), registration with medium tracking error in the images from the second row (medium SNR), and registration with low tracking error in the images from the third row (low SNR). These results can also be clearly seen in the columns D) and E) which show the fused images before registration and after registration. This shows the robustness of our algorithm.

**Lineage Analysis** - Figure 8 shows lengths of the cell lineages calculated with the proposed method, semi-automated registration, registration based on maximization of the mutual information and without registration. These results contain numbers from two different datasets; three hour dataset(G) and six hour dataset, where six or three indicate the interval between two successive imaging of Z-stacks. Longer the lineages

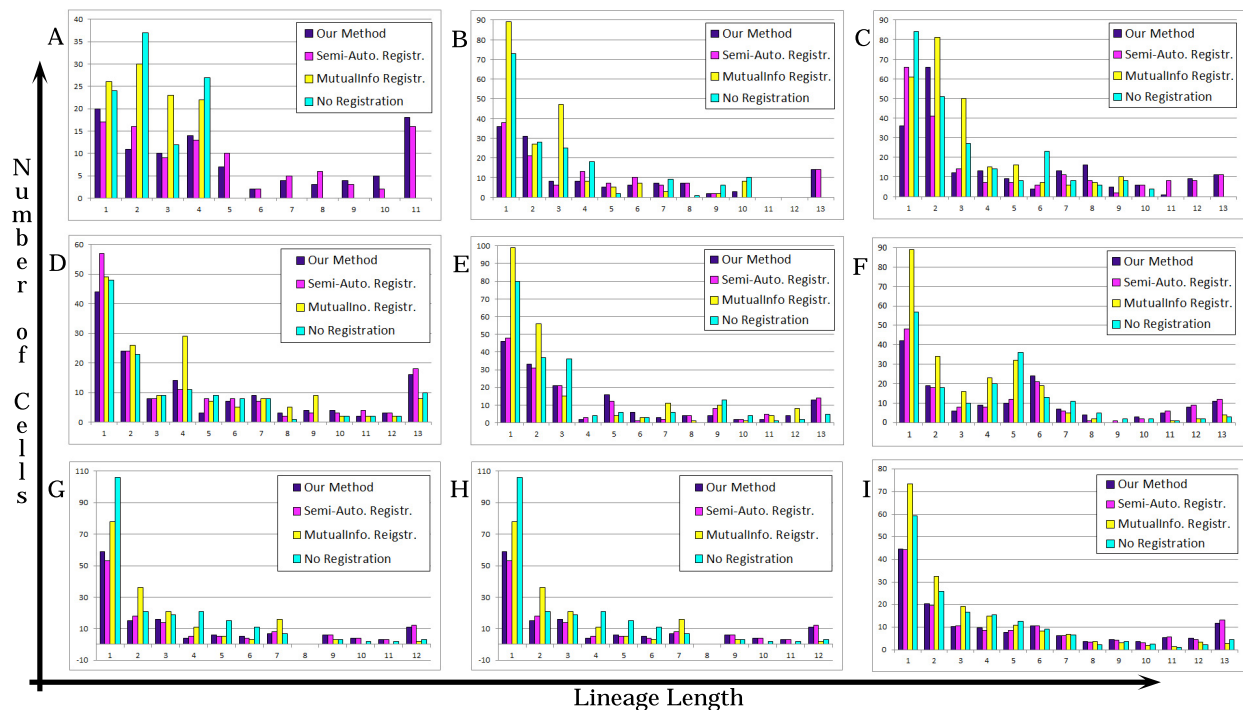


Fig. 8. Length of cell lineages for different datasets A-H. Each bar in each graph represents how many cells (number of cells) have that lineage length. I) Average length of cell lineages across all eight datasets.

are, better the results are. We can see that in tracking without registration and after registration with maximization of the mutual information, there are no cells that have lineage lengths greater than four (Figure 8 (A)), greater than eight (Figure 8 (C)) etc., as opposed to the case with the proposed and semi-automated registration, where cells have lineages for the entire 72 hours. The reason for such results is that there is a big shift between two images from consecutive time points in the middle time points. Without proper registration the tracking algorithm is not able to provide correct cell correspondence results, which interrupts the lineage of the cells. Figure 8 (I) shows the length of lineage length averaged across all eight datasets. We can see that on average we find more cells with longer lineages with our method and the semi-automated method compared to the results with registration with mutual information and without registration, where those long lineages are found in shorter peaces. Figure 8 (A) result can be also related to Figure 5 since they are representing statistics from the same dataset.

Since no cells have been tracked in frames five to six and overall there are eleven frames, then no cell can have a lineage life with the length greater than or equal to five.

Table 1 shows the number of cell divisions in 72 hours. We can see that the semi-automated and the proposed registration provide results that are close to the manual results as opposed to without registration and registration based on maximization of the mutual information.

TABLE 1  
Total Number of Cell Divisions/Ground Truth

Data	OurMethod	Semi-Auto.	MutualInfo.	NoRegistration
1	28/34	30/34	23/34	25/34
2	17/21	17/21	11/21	12/21
3	15/15	15/15	9/15	9.5/15
4	11.5/16	12.5/16	9.5/16	10/16
5	21/23	23/23	17/23	19/23
6	12.5/16	13.5/16	9/16	9.5/16

### 3.3 Discussion on the Limitations of the Proposed Method

The accuracy of the proposed image registration method depends on quality of the images and on the consistency of the cell neighborhood structure. As we have shown in our experiments, the proposed registration method can handle moderate deformations of the growing cells. However, if the deformation changes the topology of cells local neighborhood, it becomes more challenging and in some cases leads to failure of the registration module.

The image registration is acquired after the cell segmentation module, so the registration results rely on the cell segmentation results. In general in confocal microscopy based live cell imaging there could be situations where a part of the image is noisier than the other parts, especially the central regions, and hence the segmentation results sometimes are not as good as in the deeper layers. But in the proposed method we try to overcome this situation by providing landmark based registration, where it is not the entire image

that is used to do the registration. We essentially find the best points from multiple images which could be used as landmark pairs. Often these corresponding points come from the better segmented regions (clearer sections of images) and it is highly unlikely that we find a very good match in the blurred section. So the proposed method is robust to noise in part of the image and segmentation errors to a certain extent; however for a very noisy image where the segmentation is not satisfactory over the whole image the registration method is quit affected by such cases.

As shown in Figure 7, for well segmented or clearer images (Fig. 7 row 1) we have a very good registration, for not so well segmented or not so clean images (Fig. 7 row 2) we also have good registration, but where the noisy region is almost everywhere (Fig. 7 row 3) (there are more chances of finding bad landmark pairs because the nosy region is larger), we can see that the registration results are not as good as the previous cases.

Future work can consider other registration approaches to improve the results, including non-linear registration methods.

## 4 CONCLUSION

Automated image analysis such as registration, segmentation and tracking of cells in actively developing tissues can provide high-throughput and quantitative spatiotemporal measurements of a range of cell behaviors; cell expansion and cell-division kinetics, which will lead to a better understanding of the underlying dynamics of morphogenesis. In this paper, we have described an automated spatio-temporal registration method of 4D live imaging stacks of tightly packed cells, and this method is suitable across tissues which have this spatial organization of the cells in a neighborhood. The proposed registration method first finds the best image slice correspondence from consecutive image stacks. Then our proposed landmark-based registration method uses local graph-based approach to automatically find corresponding landmark pairs in the images, and finally the registration parameters computed on the selected image pairs are used to

register the entire image stack. The proposed registration algorithm combined with an existing tracking method is tested on multiple confocal image stacks of Arabidopsis shoot apical meristem and the results show that it significantly improves the accuracy of cell lineages and division statistics.

## ACKNOWLEDGMENTS

The authors at University of California, Riverside gratefully acknowledge support from NSF Video Bioinformatics IGERT grant DGE 0903667. We gratefully acknowledge Prof. Venugopala Reddy from Plant Biology at the University of California, Riverside for providing us the datasets on which results are shown.

## REFERENCES

- [1] P. Viola and M. William, *Alignment by Maximization of Mutual Information*, IJCV, 1997
- [2] M. Liu and R. Yadav et al., *Automated tracking of stem cell lineages of Arabidopsis shoot apex using local graph matching*, Plant Journal, 2010.
- [3] G.V. Reddy, M. Heisler, D. Ehrhardt and E. Meyerowitz, *Real-time lineage analysis reveals oriented cell divisions associated with morphogenesis at the shoot apex of arabidopsis thaliana*, Development, 2004.
- [4] T.F. Chan and L.A. Vese, *Active contours without edges*, IEEE Transactions on Image Processing, Volume 10, 266277 pages, 2001.
- [5] L. Vincent and P. Soille, *Watersheds in digital spaces: An efficient algorithm based on immersion simulations*, IEEE Trans. Pattern Anal. Mach. Intell., 1991.
- [6] P. Besl and N. McKay, *A method for registration of 3-D shapes*, IEEE Trans. Pattern Anal. Mach. Intell., 1992.
- [7] G.C. Sharp and S.W. Lee et al., *Invariant features and the registration of rigid bodies*, IEEE Trans. Pattern Anal. Mach. Intell., 2002.
- [8] R. Fernandez and P. Das et al., *Imaging plant growth in 4d: robust tissue reconstruction and lineaging at cell resolution*, Nat Meth, 2010.
- [9] M. Liu, A. Chakraborty, D. Singh, M. Gopi, R. Yadav, G. Reddy and A. Roy-Chowdhury, *Adaptive cell segmentation and tracking for volumetric confocal microscopy images of a developing plant meristem*, Molecular Plant, 2011.
- [10] K. Mkrtchyan, A. Chakraborty, and A. Roy-Chowdhury, *Automated Registration of Live Imaging Stacks of Arabidopsis*, International Symposium on Biomedical Imaging, 2013.
- [11] B. Cherkassky, A. Goldberg, T. Radzik, *Shortest paths algorithms: theory and experimental evaluation*, Mathematical Programming, 1996.

- [12] E.W. Dijkstra, *A note on two problems in connexion with graphs*, Numerische Mathematik, 1959.
- [13] X. Huang, B. Wang, R. Liu, X. Wang, Z. Wu, *CT-MR image registration in liver treatment by maximization of mutual information*, IEEE International Symposium on IT in Medicine and Education, 2008.
- [14] M. Bhattacharya, A. Das, *Multi resolution medical image registration using maximization of mutual information and optimization by genetic algorithm*, IEEE Nuclear Science Symposium Conference Record, 2007.
- [15] Y. Ma, J. Tian, *The Algorithm of Rapid Medical Image Registration by Using Mutual Information*, 4th International Conference on Bioinformatics and Biomedical Engineering, 2010.
- [16] F. Maes, D. Vandermeulen, P. Suetens, *Medical image registration using mutual information*, Proceedings of the IEEE, 2010.
- [17] V. Gorbunova, S. Durrleman, Lo Pechin, X. Pennec, M. de Bruijne, *Lung CT registration combining intensity, curves and surfaces*, IEEE International Symposium on Biomedical Imaging: From Nano to Macro, 2010.
- [18] Y. Zhu, S. Cheng, V. Stankovi, L. Stankovi, *Image registration using BP-SIFT*, Journal of Visual Communication and Image Representation, 2013.
- [19] A. Rangarajan, H. Chui, F.L. Bookstein, *The Softassign Procrustes Matching Algorithm*, Information Processing in Medical Imaging, 1997.
- [20] G. Li, T. Liu, A. Tarokh, J. Nie, L. Guo, A. Mara, S. Holley, ST. Wong, *3D cell nuclei segmentation based on gradient flow tracking*, BMC Cell Biology, 2007, Sep 4;8:40.
- [21] Y. Al-Kofahi, W. Lassoued, W. Lee, B. Roysam, *Improved automatic detection and segmentation of cell nuclei in histopathology images*, IEEE Transactions on Biomedical Engineering, 57(4):841-52.



**Katya Mkrtychyan** is currently a Ph.D. candidate in the department of Computer Science and Engineering at University of California, Riverside. Katya received her M.S. degree in Informatics and Applied Mathematics from the Yerevan State University, Armenia in 2008. She received her B.S. degree in Mathematics from the Yerevan State University, Armenia in 2006. Her research interests include image processing and analysis, computer vision, and bio-medical image analysis.



**Anirban Chakraborty** received his B.E. in Electrical Engineering from Jadavpur University, India in 2007 and M.S. and Ph.D. in the same subject from University of California, Riverside in 2010 and 2014 respectively. He is currently a research fellow at the Department of Diagnostic Radiology, National University of Singapore. His research interests include computer vision, pattern recognition, bio-medical image analysis, applications of probabilistic graphical models, stochastic processes and optimization in vision problems.



**Amit K. Roy-Chowdhury** received the Bachelor's degree in electrical engineering from Jadavpur University, Calcutta, India, the Master's degree in systems science and automation from the Indian Institute of Science, Bangalore, India, and the Ph.D. degree in electrical engineering from the University of Maryland, College Park.

He is a Professor of electrical engineering and a Cooperating Faculty in the Department of Computer Science, University of California, Riverside. His broad research interests include the areas of image processing and analysis, computer vision, and video communications and statistical methods for signal analysis. His current research projects include intelligent camera networks, wide-area scene analysis, motion analysis in video, activity recognition and search, video-based biometrics (face and gait), biological video analysis, and distributed video compression. He is a coauthor of two books Camera Networks: The Acquisition and Analysis of Videos over Wide Areas and Recognition of Humans and Their Activities Using Video. He is the editor of the book Distributed Video Sensor Networks. He has been on the organizing and program committees of multiple computer vision and image processing conferences and is serving on the editorial boards of multiple journals.